Mon. Not. R. Astron. Soc. **000**, 1–10 (2005) Printed 5 February 2008 (MN LATEX style file v2.2)

A fossil galaxy cluster; an X-ray and optical study of RX J1416.4+2315

Habib G. Khosroshahi[1⋆] Ben J. Maughan[2]†, Trevor J. Ponman[1] & Laurence R. Jones[1]
[1]*School of Physics and Astronomy, The University of Birmingham, Birmingham B15 2TT, UK*
[2]*Harvard-Smithsonian Center for Astrophysics, 60 Garden St, Cambridge, MA 02138, USA.*

Accepted, Received

ABSTRACT
We present a detailed X-ray and optical study of a distant fossil system RX J1416.4+2315 ($z \approx 0.137$), combining *Chandra* and *XMM-Newton* observations, optical photometry and spectroscopy. X-ray emitting hot gas imaged by both the *Chandra* and *XMM-Newton* shows a globally relaxed spatial distribution, supporting the idea that fossil groups are old galaxy systems with no recent mergers. However, the diffuse X-ray emission shows signs of asymmetries in the core of the system. With a mean gas temperature of ~ 4.0 keV and total gravitational mass of $3.1\times10^{14}M_{\odot}$, within the virial radius, this is better described as a fossil galaxy cluster rather than a fossil group. The temperature profile shows no sign of a significant cooler core despite a cooling time dropping to 5 Gyr within the resolved core. We find a mass concentration parameter $c_{200} \sim 11$ which is relatively high for a cluster of this mass, indicative of an early formation epoch.

Using the spectroscopically identified cluster members we present the galaxy luminosity function for this fossil system. We measure the velocity dispersion of the galaxies to be ~ 700 km s^{-1} based on 18 confirmed members. The dynamical mass is nearly twice the total gravitational mass derived from the X-ray analysis. The measured R-band mass-to-light ratio, within the virial radius, is ~ 440 M$_{\odot}$/L$_{\odot}$ which is not unusual for clusters of galaxies. The central giant elliptical galaxy has discy isophotes and spectral features typical of elliptical galaxies.

Key words: galaxies: clusters: general - galaxies: elliptical - galaxies: haloes - intergalactic medium - X-ray: galaxies - X-rays: galaxies: clusters

1 INTRODUCTION

Though rich clusters of galaxies are the host for giant elliptical galaxies, their high velocity dispersion is less conducive to galaxy-galaxy interactions and mergers. In contrast, smaller galaxy systems with low velocity dispersions are more merger efficient, and hence potential sites for the formation of bright and massive galaxies. N-body simulations of clusters in a hierarchical cosmological model show that galaxy merging naturally produces a massive, central galaxy with surface brightness and velocity dispersion profiles similar to observed brightest cluster galaxies. The central galaxy forms through the merger of several massive galaxies along a filament early in the cluster's history.

If a merger efficient system such as a galaxy group remains undisturbed due to relative isolation from other massive systems, a giant elliptical galaxy will form as a result of the internal multiple merger due to dynamical friction. The time-scale of such a process depends on the local density and is shorter at early formation epochs. The resulting system should lack $L^{\star}$ galaxies but the fainter end of the luminosity function should remain intact, as only a small fraction of the accreted mass is due to the dynamical friction of smaller galaxies over a Hubble time (Dubinski 1998). With highly relaxed intra-group hot gas revealed by X-ray observations and a gap of at least 2 magnitude between the first and second ranked galaxies (Jones et al. 2003), galaxy groups known as "fossil groups" appear to be the observed products of the above mechanism (Ponman et al. 1994).

There are about a dozen such systems identified (Ponman et al. 1994; Vikhlinin et al. 1999; Mulchaey & Zabludoff 1999; Jones et al. 2000; Romer et al. 2000; Matsushita 2001; Jones et al. 2003) but few of them have been studied in detail (Khosroshahi, Jones & Ponman 2004; Sun et al. 2004). Based on the space density of fossils, Jones et al. (2003) estimate that fossil systems represent 8%-20% of all galaxy systems with the same X-ray luminosity, and are as numerous as poor and rich clusters combined. Therefore they account for a significant fraction of the galaxy systems in the universe, though observationally they are difficult to find, especially at higher redshifts.

⋆ E-mail: habib@star.sr.bham.ac.uk
† Chandra Fellow

About half a dozen fossils have been studied in the X-ray where they are most impressive. The nearest known fossil group NGC 6482, for instance, has shown interesting properties (Khosroshahi, Jones & Ponman 2004), such as an unusually high mass concentration and absence of a cooler core despite the very short cooling time. Sun et al. (2004) studied a more massive fossil using *Chandra* and *XMM-Newton* , and find a much smaller cool region than expected. If our arguments about the early formation epoch of the fossils are correct, these systems should be ideal laboratories to study cool cores. This is because of the absence of an obvious cooling flow removal mechanism, major cluster merging, and therefore other heating mechanisms can be looked into with less ambiguity.

Fossils groups are equally important in their optical properties, as they provide a suitable environment to study the stellar properties of giant elliptical galaxies. Fossils are isolated and old systems enabling us to make a direct comparison between the morphology of ellipticals grown in fossil groups and their counterparts at the core of galaxy clusters. This is further motivated by an earlier finding that there are enough fossils, from their space density, to provide the giant dominant ellipticals in clusters. There is a need for detailed optical studies to address various issues such as the mass-to-light ratio and luminosity function of galaxies, in addition to X-ray studies. The central galaxy warrants special attention, as the age of its stellar population can provide further clues to the cluster history, complementing the X-ray studies.

This paper is organised as following: Section 2 briefly reviews the group properties and describes the observations, data reduction and preparations. The results from imaging and spectral X-ray analysis are presented in section 3. Section 4 describes the distribution of mass. Results from optical and near-IR photometry, optical spectroscopy and mass-to-light ratio are presented in section 5. A discussion and concluding remarks are summarised in section 6.

We adopt a cosmology with $H_0 = 70$ km s^{-1} Mpc^{-1} and $\Omega_m = 0.3$ with cosmological constant $\Omega_\Lambda = 0.7$ throughout this paper. At the redshift of RX J1416+2315 the luminosity and angular diameter distances are 650 Mpc and 500 Mpc, respectively and 1 arcsec $\equiv$ 2.44 kpc.

2 OBSERVATION AND PREPARATION

2.1 The group:

The group RX J1416.4+2315 (hereafter J1416), $z \approx 0.137$, was first studied as part of a volume limited sample of spatially extended X-ray sources compiled during the WARPS project (Wide Angle ROSAT Pointed Survey; (Scharf et al. 1997; Jones et al. 1998; Perlman et al. 2002)). Details of the initial sample selection and the search leading to the volume limited sample of fossil groups can be found in Jones et al. (2003). It is the most X-ray luminous source in the sample of 5 fossil groups studied by Jones et al. (2003), with a ROSAT estimated X-ray bolometric luminosity of 1.1×10^{44} erg s^{-1}. In a deep optical image it would be classified as a galaxy group or poor cluster centred on an extremely dominant, luminous giant elliptical galaxy. The very extended X-ray emission is detected to a semi-major axis length of 3.5 arcmin (512 h_{70}^{-1} kpc) in the ROSAT PSPC (Position Sensitive Proportional Counter) and is elongated in a direction similar to that of the central elliptical galaxy.

This galaxy cluster appears in the bright SHARC cluster survey of Romer et al. (2000). The redshift is confirmed, but it is not identified as a fossil system by Romer et al. (2000). The target of this ROSAT field was a candidate cluster of galaxies, but at a high redshift (z$>$ 0.3), and unrelated to the fossil system.

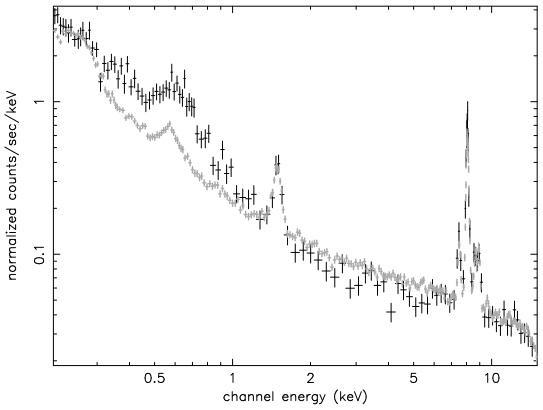

Figure 1. Background spectra obtained from the source field (black) and blank sky dataset (grey). The blank sky spectrum was normalised by the flux of events detected outside the field of view.

The VLA FIRST catalog of radio sources gives a radio source at the centre of the giant elliptical galaxy with an integrated flux of 3.39 mJy at 1.4 GHz. The radio source is extended on a scale of 4 arcsec.

2.2 *Chandra* observations

The *Chandra* observation of this group was performed in September 2001 (Obs ID 2024) for a total of 14.8 ks using *Chandra* ACIS-S. No major flares were detected therefore an exposure of 14.5 is used in the analysis. Though this observation helps to detect and position the point sources with a high spatial accuracy and gives enough counts to study the global properties such as the spatial distribution and the core temperature of the hot gas, it does not provide enough counts for a more detailed analysis out to a large radius.

We follow the same procedure as Khosroshahi, Jones & Ponman (2004) for the *Chandra* analysis except that we use a later version of the analysis tools (CIAO 3.2 and CALDB 3.0). We therefore correct for the quantum efficiency degradation of ACIS, which increases with time. We use CTI corrected blank-sky background files in our imaging and spectral analysis as the ACIS-S3 chip is contaminated by the source emission due to the large extension of the X-ray halo. To study the soft diffuse X-ray emission, point sources were detected using CIAO "wavdetect" and removed. Their locations were then filled with surrounding background using a linear interpolation. A total of 20 point sources were detected. The brightest point source was an off-centre background AGN at 14:16:24.7, +23:16:14.9 (J2000).

2.3 *XMM-Newton* observations

The large collecting area and field of view of *XMM-Newton* make the *XMM-Newton* observations attractive despite relatively poor spatial resolution compared to that of *Chandra* . The system was observed by *XMM-Newton* for 28ks in July 2003. The observation was split into two parts of 19ks and 9ks. The data were reduced and analysed with version 6.1 of the Science Analysis System (SAS) and with the most recent calibration database as of January 2005.

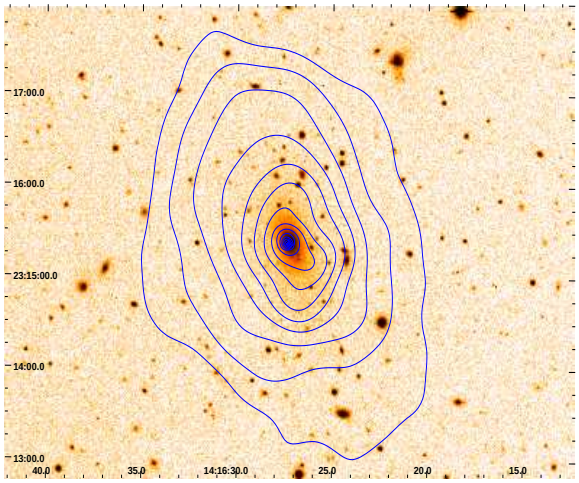

Figure 2. X-ray contours from the soft (0.3-2.0 keV) diffuse, point sources removed, X-ray emission detected by *Chandra* are overlaid on a 6×6 arcmin^2 size deep R-band optical image.

The 19ks observation was rendered completely unusable by extremely high background levels, though the second interval was mostly unaffected by high background periods. After cleaning, there were 8ks and 4ks of good time for the MOS and PN cameras respectively. Blank sky background datasets (Read and Ponman 2003) were also prepared and cleaned in the same way.

The reasonably small size of the source on the EPIC detectors meant that there was sufficient local background data to enable useful comparisons to be made with the blank sky background fields to determine their suitability for data analysis purposes for this dataset. The spectrum of the background in the observation was compared to that in the blank sky data, after normalising them by the particle background flux measured from the events detected outside the field of view of the telescopes. The resulting background spectra are plotted in Fig 1 for the PN detector (the MOS spectra are similar).

There is a significant excess in the source dataset at the soft end, due to higher Galactic X-ray background at the source position. The normalisation of the continuum above 2 keV is too high in the blank sky background, but the normalisation in the particle-induced fluorescent lines (1.5 and 8 keV) is correct. This means that the ratio of particle to hard X-ray background flux in the source data set is higher than that in the blank sky background. When the blank sky spectrum is normalised by the particle background flux, the other background components are overestimated, giving rise to a higher continuum level.

This result suggests an alternative method of normalising the blank sky background; using the $2-7$ keV flux. The upper limit is imposed to avoid another fluorescent line complex in the PN data. This method gives the correct >2 keV continuum, but underestimates the fluorescent line flux. The effect of these two methods on temperature measurements is discussed later.

2.4 Optical photometry and spectroscopy

The imaging and spectroscopic observations of the group was performed using the observational facilities of the Issac-Newton Group of Telescopes (ING), Kitt-peak National Observatory (KPNO) and UK Infrared Telescope (UKIRT). The R-band image was obtained using the INT 2.5m wide field imager during a service time observation in August 2000. Unfortunately the conditions were not photometric, so further R-band imaging was obtained with the 8k mosaic camera at the University of Hawaii 2.2-m telescope in photometric conditions, and used to calibrate the original images.

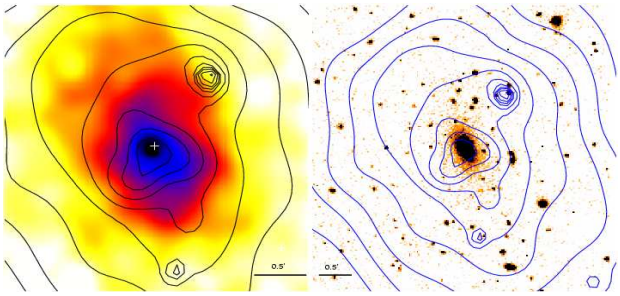

Figure 3. X-ray soft (0.5-2 keV) diffuse emission contours from *XMM-Newton* overlaid on *Chandra* soft diffuse X-ray emission (left) and the R-band image of the central galaxy (right). Both the *Chandra* and *XMM-Newton* show asymmetries in the core. The white cross shows the location of the radio source from the FIRST catalog and matches the position of a point source detected at the centre of the cluster.

The spectroscopic observations were performed during a run to study several fossil groups using a multi-slit spectrograph on the KPNO-4m telescope on the 11-13th March 2000. The Ritchey-Cretien spectrograph and KPC-10A grating gave a dispersion of 2.75 $\AA$/pixel over 3800-8500 $\AA$ and with 1.8 arcsec slitlets a resolution of $6\AA$ (FWHM) was achieved. Risley prisms compensated for atmospheric dispersion. Spectra were obtained through three slitmasks, with typically an hour exposure on each. The spectroscopic data were reduced and analysed in the standard way using IRAF.

The high quality near infrared images of the target were obtained in June 2004 using UIST/UKIRT. Data reduction was performed using the Observatory Reduction and Acquisition Control (ORAC) data reduction tool and four 180 sec exposure mosaic images were then combined to increase the signal-to-noise.

3 X-RAY ANALYSIS AND RESULTS

3.1 Spatial distribution

Figure 2 shows the contours of soft (0.3-2.0 keV) diffuse X-ray emission from the *Chandra* observation on R-band optical image. The contours extended to 500 kpc along the semi-major axis of the X-ray emission. They appear relaxed and aligned with the stellar major axis of the giant elliptical galaxy.

The *XMM-Newton* soft (0.5-2 keV) diffuse X-ray emission contours are also shown (Fig. 3). The diffuse emission image was produced by adaptively smoothing an exposure-corrected image of the emission detected by the three *XMM-Newton* EPIC cameras to 99% significance. Unlike Fig. 2, here the point sources are not excluded. The off-centre AGN can be seen just North-West of the centre of the X-ray emission. The X-ray emission from the system at this energy range appears relaxed, overall, except in the core, where asymmetries are seen. The *Chandra* diffuse emission of the core shows a NE-SW elongation and a SW 'tail' (Fig. 2) which are also seen in the *XMM-Newton* contours (Fig 3). However, some of the other irregularities seen in the *XMM-Newton* image are not apparent in the *Chandra* data.

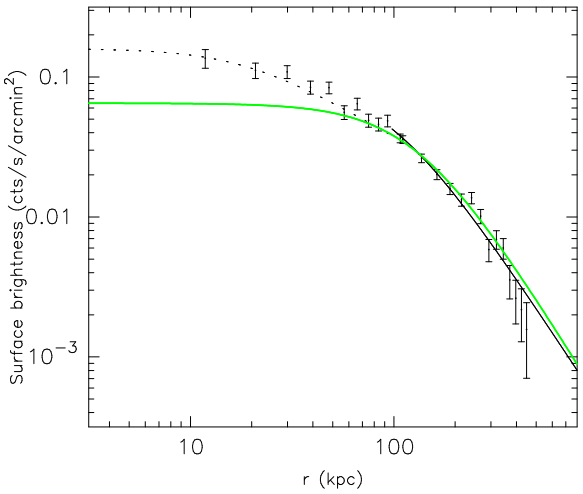

Figure 4. Radial surface brightness profile and the double β-model fit to the soft energy (0.3-2.0 keV) X-ray emission from *Chandra* . The dotted curve is the β-model fit to the inner region, $\sim$100 kpc. The dark solid curve is the β-model to the outer region. The thick gray (green) curve represents the β-model fit to the *XMM-Newton* surface brightness profile.

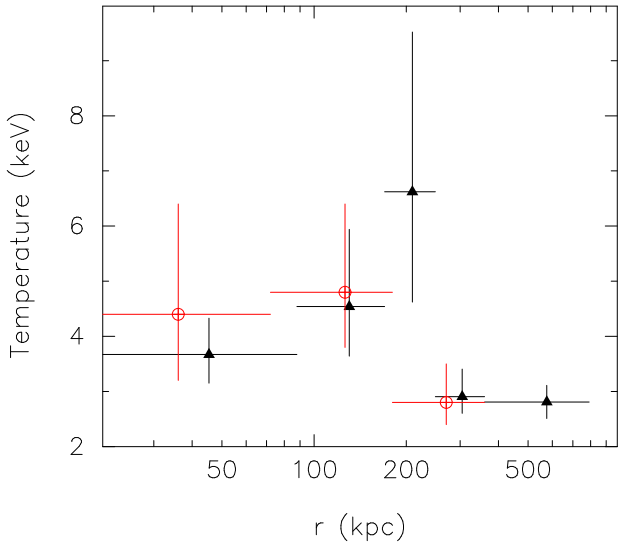

Figure 5. Temperature profile of J1416. The triangles (black) show the de-projected temperature profile from *XMM-Newton* analysis and the circles (red) is the same from *Chandra* analysis.

3.1.1 *Surface brightness distribution*

A radial surface brightness profile (Fig 4) was extracted from the inner 200 arcsec of the ACIS-S3 image in a soft energy range (0.3-2.0 keV) and fitted by a one-dimensional β-model,

$$\Sigma(r) = \Sigma_0[1 + (\frac{r}{r_0})^2]^{-3\beta+1/2}, \quad (1)$$

where r_0 and β are the core radius and index, and Σ_0 the central surface brightness. This gives a core radius of r_0= $28.2^{+5.14}_{-4.43}$ arcsec and β=$0.47^{+0.03}_{-0.02}$ but is far from a good fit to the data.

With the clear ellipticity in the two-dimensional X-ray distribution and larger area covered by *XMM-Newton* EPIC we performed a two dimensional β-model fit to the MOS 1, MOS 2 and PN images at the same energy band. The core radius along the major axis is $r_0 = 54 \pm 4$ arcsec, with $\beta = 0.54 \pm 0.02$ and ellipticity of 0.34 ± 0.06. A two-dimensional β-model fit to the *Chandra* data gives a $r_0 = 36 \pm 3$ arcsec and $\beta = 0.44 \pm 0.01$ with an ellipticity of 0.36.

There is a large difference in the values of β and the core radius obtained from *Chandra* and *XMM-Newton* analysis. To find the root of the discrepancy and also because of a relatively poor fit to the *Chandra* data we performed a double-β fit by fitting inner and outer regions of the image each with a single β-model. The parameters of these β-models are, however, tied to give a continuous gas density (Khosroshahi, Jones & Ponman 2004; Pratt & Arnaud 2003) at the break radius, 100 kpc. We find r_{0in}= $7.7^{+3.3}_{-3.1}$ arcsec and β_{in}=$0.31^{+0.06}_{-0.03}$ and r_{0out}= $37.0^{+4.1}_{-4.3}$ arcsec and β_{out}=$0.53^{+0.02}_{-0.02}$ with a reduced χ^2=1.32. Fig 4 shows this β-model fit and the β-model fit to the *XMM-Newton* surface brightness profile.

3.2 Spatially resolved spectroscopy

3.2.1 *Chandra*

The ACIS spectra in three successive circular annuli were extracted and fitted with a de-projected (using XSPEC projct model) absorbed APEC (Smith et al. 2001) model. A fixed hydrogen column density of $N_{H,gal} = 2 \times 10^{20}$ cm^{-2} was included in the model to account for Galactic absorption. The background was extracted for each annulus from the blank sky observations in the same detector regions as the source spectra. Each spectrum contains about 1000 counts in bins of 20 counts each. Since we were not able to estimate the metallicity from the spectral fits, we fixed the metallicity to 0.5 $Z_\odot$, the mean value from *XMM-Newton* analysis on a similar scale.

The unabsorbed flux from the central 200 arcsec is 1.22×10^{-12} erg s^{-1} cm^{-2}, which corresponds to an X-ray luminosity, 1.04×10^{44} ergs/s (0.5-8.0 keV) and a bolometric luminosity of 1.24×10^{44} ergs/s. The fitted column density was found to be consistent with the galactic level, though poorly constrained with an error of about 0.1×10^{22} cm^{-2}.

3.2.2 *XMM-Newton*

Spectra were extracted from 5 circular annular regions defined to contain $\geq$ 1200 source counts. The effect of different background subtraction methods on the measured temperatures was investigated. A local background spectrum was extracted from an annular region free from source emission. A background spectrum was extracted from the blank sky background in the same detector region as the source spectrum, and was corrected for the residuals between the local and blank sky backgrounds using the "double subtraction" method described by (e.g. Arnaud et al. (2002)). These two methods were also repeated with the events weighted (using evigweight) to correct for the telescope's vignetting. This weighting has the disadvantage of incorrectly boosting the non-vignetted particle background component. The two blank sky methods (i.e. with and without weighting) were performed with the blank sky background normalised by either the flux of events detected outside the field of view of the telescopes or using the 2-7 keV flux. This gives a total of 6 background subtraction methods.

The spectra from each detector were grouped to contain $\geq$ 20 counts per energy bin, and were fit simultaneously in the 0.4-7keV band by an absorbed APEC model. The absorbing column was fixed at the Galactic value as before, and the temperature, metal abundance and normalisation were free parameters in the fit. The temperature and metallicity of the PN and MOS spectral models

were tied together, but the normalisations were allowed to fit independently.

The temperature profiles obtained with the non-weighted methods were found to be in excellent agreement, regardless of background subtraction method. However, the methods using weighted spectra were less consistent. As one might expect, the dispersion of temperatures increased with radius, as the background becomes more important. The agreement between the non-weighted methods is excellent at all radii, while the temperatures measured with the (evig) weighted methods become inconsistent with each other, and the non-weighted methods at larger radii. This is perhaps unsurprising, as we have already seen that the non-vignetted particle background in the source dataset is relatively high (section 2.3). Based on these results, we chose to use the non-weighted, local background method for all of the *XMM-Newton* spectral analysis.

The surface brightness distribution of J1416 is clearly elliptical, so the effect of this on the measured quantities such as the temperature profile is investigated by extracting spectra in elliptical annuli. The ellipses were chosen to closely match the isophotes, and contain ~ 1200 source counts. The resulting temperature profile was consistent with that measured with circular annuli, and so the circular temperature profile is used throughout for consistency with our assumption of spherical symmetry in estimating the mass of the system.

With the methodology thus established, the temperature profile was deprojected using the XSPEC projct model. Similarly we obtained a PSF-deconvolved temperature profile, however due to limited statistics we were unable to constrain the temperatures with the choice of bin sizes described above which is the largest to enable us perform a mass profile analysis. We therefore did not use the PSF-deconvolved temperature profile for this study.

3.3 Temperature and metallicity

Fig 5 shows the deprojected temperature profile of the cluster based on various analysis methods out to 4 arcmin ($\sim$ 700 kpc). The *XMM-Newton* temperature agrees with the overall temperature found from *Chandra* observations of the central 130 kpc. Within the resolution of the data we find no significant drop in the temperature of the central annulus, in contrast to the observed temperature profiles of many relaxed clusters of galaxies which present cool cores (Vikhlinin et al. 2005).

With limited counts from *Chandra* observations, our estimation of the metal abundances are based on the *XMM-Newton* observations, however, the deprojected metallicities are very poorly constrained. The mean metallicity, within 400 kpc, is found to be 0.23$\pm$0.076 solar metallicity.

3.4 Gas entropy and cooling time

The entropy of the X-ray emitting gas is defined here as:

$$S(r) = kT(r)/n_e(r)^{2/3}\,\mathrm{keVcm}^2, \quad (2)$$

where n_e is the electron density. The shape of the entropy profile is of special interest since preheating models predict large isentropic cores. Using the β-model fit to the surface brightness profile and the central gas density, obtained from the spectral fit, we can derive an analytical relation for the gas entropy providing that we model the temperature profile using an analytical function. Two entropy profiles shown in Fig 6 are obtained in this way by assuming

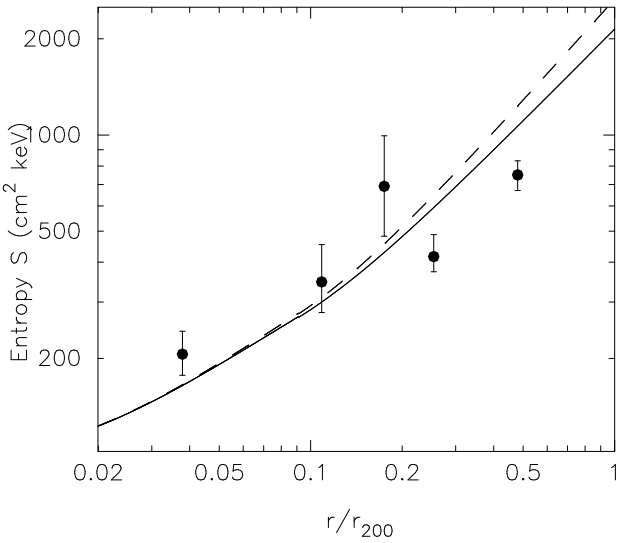

Figure 6. Entropy profile of the hot gas in J1416. The data points are obtained from emission measure for each annulus with its associated temperature. Solid and dashed lines are the entropy profiles assuming polytropic and isothermal temperature profiles, respectively.

isothermality ($T \approx 4.0$ keV) and a polytropic fit ($\gamma = 1.1$) to the temperature profile. In addition we obtain the gas entropy in each spherical shell (data points in Fig 6) by estimating the electron density via the emission measure assuming a Raymond-Smith plasma emission model for each spherical shell and the L is the X-ray luminosity from the shell with the volume V. The gas entropy at $0.1r_{200}$ (see section 3.5.1 for estimate of r_{200}) is $S_{0.1} \approx 300 \pm 50$ keV cm^2 similar to the average value obtained by Ponman et al. (2003) for clusters with similar temperatures. No isentropic core is seen, though our spatial resolution is limited. This is consistent with other examples of group and cluster scale systems reported to show no large isentropic cores (Pratt & Arnaud 2003; Ponman et al. 2003).

The cooling time of the gas was calculated by dividing the total thermal energy of each shell by the associated emissivity, $t_{cool} \sim \frac{3}{2}\frac{(n_e+n_H)kT}{\epsilon}$, where ϵ is the bolometric emissivity obtained by assuming a Raymond-Smith plasma emission model. The resulting profile is presented in Fig 7.

3.5 Gas and total gravitational mass profiles

The gas mass and the total gravitational mass profile can be derived from the gas density and the temperature profiles assuming that the gas is in hydrostatic equilibrium and is distributed with spherical symmetry. To support our assumptions we note that the distribution of the hot gas in this system is fairly symmetric and regular with the exception of a small region in the core. In addition, the comparison between the temperatures from circular and elliptical shells shows no significant difference in this case. The *Chandra* analysis of the X-ray surface brightness distribution shows that there is no significant discrepancy in the results of the surface brightness profile by performing a one-dimensional analysis by selecting circular annuli or a two-dimensional fit. Finally Fabricant et al. (1984) show that the mass profile, from X-ray analysis, of an oblate or prolate system is similar to the one obtained under spherical symmetry assumption.

The total gravitational mass is given by:

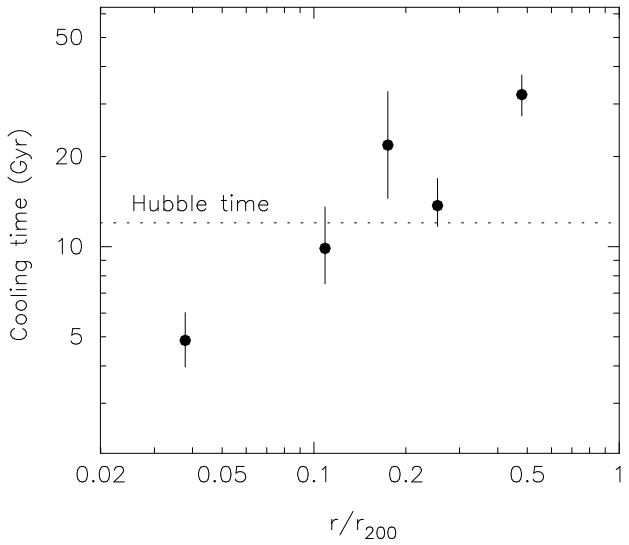

Figure 7. The estimated cooling time for each shell. The resolved core has a cooling time $\sim$ 5 Gyr, yet we observe no cooler core in the temperature profile.

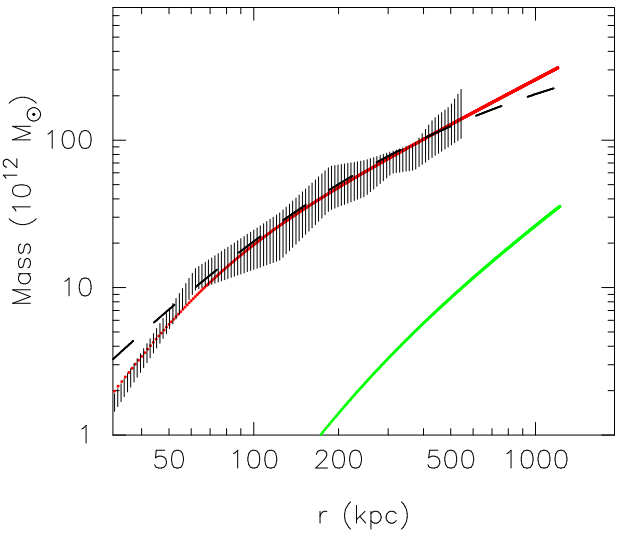

Figure 8. Total gravitational mass and gas mass profiles of J1416. The upper solid (red) curve shows the gravitational mass profile. The dashed curve represents the NFW profile. The error envelope of the total gravitational mass is shown with vertical hashes. The lower solid (green) curve shows the gas mass profile. The concentration parameter is $c_{200} = 11.2 \pm 4.5$. The mass data points and errors are those estimated using MC simulations.

$$M_{grav}(< r) = -\frac{kT(r)r}{G\mu m_p}\left[\frac{dln\rho(r)}{dlnr} + \frac{dlnT(r)}{dlnr}\right]. \quad (3)$$

where G and m_p are the gravitational constant and proton mass and $\mu = 0.6$.

The temperature profile seen in Fig 5 is modelled by a polytropic model with β and core radius fixed to the values obtained from the surface brightness fit to the *Chandra* data giving $\gamma \simeq 1.09$. It is then straightforward to derive an analytical description for the total mass using the expressions for density under the polytropic assumption. However the error in the mass should be obtained indirectly. We use a Monte-Carlo method which is described in Khosroshahi, Jones & Ponman (2004) and Neumann & Böhringer (1995) for our error estimation. In brief, the formula for the mass profile consists of two parts, the variation in gas density ($d\ln n/d\ln r$) and in the temperature ($T(r)$ and $d\ln T/d\ln r$). For the latter we have generated 1000 physical temperature profiles with a temperature envelope defined by the observed errors in the temperature and linear interpolation. A physical temperature profile is one which guarantees a monotonically increasing mass with radius. In this simulation the density profile parameters were fixed at the values from the β-model fit. In order to estimate the contribution of the density variation ($d\ln n/d\ln r$) to the mass error, the surface brightness profile at the location of each data point was fitted with $d\ln n/d\ln r$ as the free parameter instead of β. The error was estimated at the 68% confidence level using the error matrix provided by the fitting program. We checked the results by monitoring the χ^2 variation. The total error in the mass at each data point was then derived by adding the two uncertainties quadratically.

3.5.1 *NFW mass profile and concentration*

Motivated by the results of numerous cosmological N-body simulations and to enable us to make a direct comparison with mass profiles from other studies, we attempt to fit a NFW profile (Navarro et al. 1995)

$$\rho_m(r) = \frac{4\rho_m(r_s)}{(r/r_s)(1+r/r_s)^2}, \quad (4)$$

to the total gravitational mass density. Integrated the mass profile for a spherical mass distribution leads to,

$$M_{tot}(< r) = 16\pi\rho_m(r_s)r_s^2[r_s \ln(1+r/r_s) - \frac{r}{1+r/r_s}], \quad (5)$$

where $\rho_m(r_s)$ is the density at r_s. The mass concentration parameter can then be defined as $c_{200} = r_{200}/r_s$. By definition, r_{200} is the radius within which the mean gravitational mass density is 200 times the critical density, $\rho_c(z)$. For our assumed cosmology (Ω_m=0.3, Λ=0.7), the critical density is $\rho_c(z) = \frac{3H_0^2}{8\pi G}(1+z)^2(1+z\Omega_m)$.

We fit the NFW mass profile (equation 5) to the five observed data points with errors obtained from MC simulation. The best fit profile has $r_s = 97$ kpc. r_{200} is then calculated by extrapolating the profile to $200\rho_c$. This gives $r_{200} = 1.22 \pm 0.06$ Mpc. The extrapolated total mass, using the best fit NFW profile, at r_{200} is $M_{200} = 3.1(\pm 1.0) \times 10^{14}$ M$_\odot$.

To obtain the concentration of the dark matter we take into account the contribution of the stellar mass of the central dominant galaxy, for which we have the R-band luminosity and assume a stellar M/L$_R$ $\sim$ 5 M$_\odot$/L$_\odot$ from the recent fundamental plane studies (Cappellariet al. 2005). This gives $r_s = 108$ kpc and therefore a concentration parameter $c_{200} = 11.2 \pm 4.5$, which is high compared to the values of c_{200} for poor clusters studied by Pratt & Arnaud (2005). Implications of this high mass concentration is discussed in section 5.

The integrated gas mass can be derived by integrating the gas density. Fig 8 shows the gas mass profile. The total gas mass within r_{200} is $\sim 4 \times 10^{13}$ M$\odot$. With the extrapolated total gravitational mass within the same radius $\sim 3.1 \times 10^{14}$ M$\odot$, the gas fraction is calculated to be ~ 0.13.

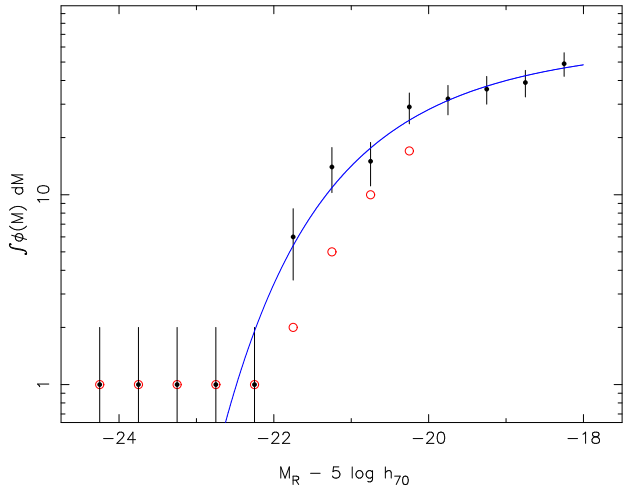

Figure 9. Galaxy luminosity function of J1416. The dark data points and the associated error bars show the luminosity function of the galaxies using a statistical subtraction of the background using two regions outside the virial radius. The curve (blue) is the best fit Schecter function to these data points. The open circles (red) represent the luminosity function of the the confirmed cluster members.

4 OPTICAL PHOTOMETRY AND SPECTROSCOPY

To estimate the completeness of our spectroscopic observation we extract galaxies down to $R = 19.5$ mag using Sextractor. This gives a total of 48 sources within $0.5r_{200}$ (the radius used in the definition of fossil systems by Jones et al. (2003)), of which 9 are classified as stars. From the total of 39 galaxies, only 27 were observed, of which 18 were cluster members with a mean redshift of 0.137 and calculated galaxy velocity dispersion of $\sigma = 700 \pm 120$ km s^{-1}. Some of the galaxies (8 in total) have been missed due to the slit configuration. Four galaxies were know to be foreground galaxies prior to this observation. We estimate the completeness of the sample to be 77 percent within $0.5r_{200}$ and down to $m_R = 19.5$. Based on this calibration, the magnitude of the central galaxy is 15.17 and the second brightest galaxy in the cluster is $m_R = 17.7$. None of the galaxies missed due to the slit configuration were brighter than $R = 17.7$, thus the system does meet the formal fossil criteria of Jones et al. (2003).

4.1 Luminosity function

The luminosity function (LF) of galaxies in this fossil cluster is obtained by selecting the galaxies down to M_R ∼-18.5. The cumulative LF is shown in Fig 9 after statistical subtraction of the background galaxies extracted from two fields around the source just outside the r_{200} of the cluster. In this figure we show the luminosity function of the spectroscopically confirmed cluster members (open red circles) and the luminosity function of galaxies (filled circles) after a statistical subtraction of the field galaxies and the associated error bars.

Fitting a Schecter function to the LF of confirmed members, we obtain $\alpha = -1.23 \pm 0.28$ and $M_R^\star = -20.40 \pm 0.22$. An independent study of a higher quality galaxy sample for this fossil cluster results in a similar slope (Cypriano, Mendes de Oliveira & Sodre Jr. 2006). We obtain $\alpha = -0.61 \pm 0.20$ and $M_R^\star = -20.55 \pm 0.40$ when we fit a Schecter function to the LF of photometrically selected galaxies (solid curve in the Fig 9). As this figure shows, this luminosity function is considerably shallower. There is an inconsistency in the slopes of the galaxy luminosity functions of the confirmed members and that obtained from statistical background subtraction, which could be due to the fact that the statistical background subtraction is performed based on the galaxy classification, using SExtractor, in the absence of galaxy colours.

For RX J1552.2+2013, another fossil with a similar mass to J1416, Mendes de Oliveira, Cypriano & Sodre Jr. (2005) find a slope of $\alpha = -0.77 \pm 0.37$ for the spectroscopically selected galaxies and $\alpha = -0.64 \pm 0.30$ for the photometrically selected galaxies. From the study of the GEMS X-ray groups, Miles et al. (2004) find $\alpha = -1.0$. They also report a dip in the luminosity function which is more prominent in poor groups and is argued to be the result of galaxy mergers in groups. A similar mechanism is thought to be the origin of the large gap in fossils' luminosity function. This is discussed in section 5.

4.2 Mass to light ratio

Having the total gravitational mass and the optical luminosity of the cluster we are in a position to estimate the mass-to-light ratio of the system.

The total R-band luminosity of the cluster is measured to be $10^{11.85}\ L_\odot$ by accumulating the luminosity of the photometrically identified cluster members within r_{200}. Thus the total mass-to-light ratio within r_{200} is $\sim 440\ M_\odot/L_\odot$. Converting this to the mass-to-light ratio in B-band we find $M/L_B \sim 580\ M_\odot/L_\odot$. This M/L, derived assuming B-R=1.5, is an upper limit because all the cluster galaxies are assumed to be early-types. Under a similar assumption Mendes de Oliveira, Cypriano & Sodre Jr. (2005) find a mass-to-light ratio of $M/L_B \sim 750\ M_\odot/L_\odot$ for another massive fossil based on a dynamical mass estimate. These mass to light ratios, ours and that of Mendes de Oliveira, Cypriano & Sodre Jr. (2005), are relatively high compared to the results of distant clusters $M/L_R \sim 210 M_\odot/L_\odot$ (Carlberg et al. 1996; Girardi et al. 2002). However, higher values of mass to light ratio are also reported (Mohr et al. 1996). In comparison to other fossils (Vikhlinin et al. 1999; Yoshioka et al. 2004) these fossils and NGC 6482 (Khosroshahi, Jones & Ponman 2004) have lower mass-to-light ratio and hence difficult to argue whether or not fossils have, in general, higher values of M/L.

4.3 The central galaxy

To study the stellar light distribution of the central giant elliptical galaxy we performed an isophotal analysis using the high resolution UIST K-band images of the system. The isophotal analysis using the IRAF task 'ellipse' shows a discy nature for the stellar light at an outer radius of $r > 20$ kpc as shown in figure Fig 10. The ellipticity of the galaxy increases to a value of 0.43, overtaking the ellipticity of the X-ray distribution as expected (Buote & Canizares 1996). To find out if this is a pure elliptical galaxy we fitted a Sersic profile ($r^{1/n}$) to the radial surface brightness profile using a two dimensional decomposition technique which allows for a possible disc component, with an exponential profile. We find no disc contribution to the total galaxy light. We find a Sersic index of $n \sim 3.0$ and a half light radius of ~ 20 kpc. The giant elliptical galaxies in galaxy clusters often show boxy isophotes (Bender, Burstein & Faber 1992) while having larger values of n (Khosroshahi et al. 2004). Further discussion should be based on a well defined sample of dominant galaxies in fossils, which is the subject of a separate study.

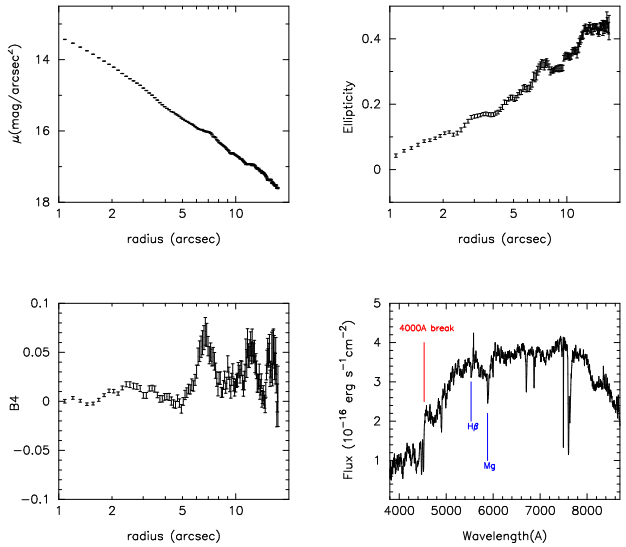

Figure 10. Isophotal analysis of the central galaxy in K-band. Surface brightness radial profile (top-left), ellipticity profile (top-right), Cosine coefficient B4 (bottom-left) and the stellar spectrum of the giant elliptical galaxy are presented.

The spectrum of the central galaxy is similar to that of a typical elliptical galaxy, with $H\beta$ and Mg lines marked in Fig 10.

5 DISCUSSION AND CONCLUSIONS

Using the high angular resolution of the *Chandra* and higher sensitivity of the *XMM-Newton* , combined with optical imaging and spectroscopy and near IR imaging, we studied the most massive and hot fossil galaxy system, which also hosts the the most luminous giant elliptical galaxy observed in fossils.

We confirm the result of an earlier ROSAT study that RX J1416.4+2315 meets the requirements of being a "fossil" discussed in Jones et al. (2003). These are the minimum X-ray luminosity of 10^{42} erg s^{-1} and a minimum of two magnitude difference in R-band luminosity between the two brightest galaxy belonging to the system (within $0.5r_{vir}$). The examination was necessary as the gas temperature in the earlier study was underestimated by $\sim 40\%$ resulting in a smaller virial radius within half of which we had to examine the above optical criteria.

The global X-ray distribution is relaxed, except a small region at the core, indicating an absence of any recent group-group merger and major galaxy-galaxy merger indicative of an early formation epoch. The central dominant galaxy is a giant elliptical galaxy aligned with the X-ray emission and hence the dark matter distribution. The alignment which is also seen in NGC 6482 (Khosroshahi, Jones & Ponman 2004) and ESO 3060170 (Sun et al. 2004) is an interesting feature which is known to be the consequence of an anisotropic collapse, such as along a filament. The alignment effect only works for the central giant elliptical galaxy and is seen in the N-body simulations (Dubinski 1998). Recent hydrodynamical cosmological simulations, to investigate the effect of baryonic dissipation on halo shapes (Kazantzidis, Zentner & Nagai 2005), show that there is also a strong correlation between dark matter halo shape and stellar remnant morphology in collisionless mergers.

Despite the high degree of relaxation and symmetry, there are signs of asymmetry at the core of the system. These are seen in the X-ray soft emission within the core. This could be a result of AGN activity. VLA FIRST catalog gives the integrated flux of the central AGN in the giant elliptical galaxy as 3.39 mJy at 1.4 GHz, with a spatial size of 4 arcsec. Radio observations of the system are currently being performed to investigate the detailed morphology of the radio emission and the status of the AGN duty cycle.

If fossil groups are old systems, as argued, they should provide ideal environments for the formation of cool cores, due to the absence of any recent major merger which can remove the cool core. The temperature profile shows no significantly cooler core, suggesting the existence of a heating mechanism. Given the limited statistics and the *XMM-Newton* point spread function, the presence of a small (< 50 kpc) cooler region cannot be ruled out. However the absence of cool core is also found in the case of the nearest observed fossil, NGC 6482 (Khosroshahi, Jones & Ponman 2004) where the core is resolved with 1 kpc resolution. In addition ESO 3060170 (Sun et al. 2004) shows a cool core much smaller than the expected cooling region for a system of few 10^{14} $M_{\odot}$. As mentioned above there is evidence of AGN activity in the core of RX J1416+2315, similarly to ESO 3060170.

This study shows that the X-ray temperature from a previous ROSAT study was underestimated by about half its value. It is therefore important to study the effects of these changes on the scaling relations involving X-ray quantities. This is the subject of a separate study concentrating on the X-ray scaling relations of fossil galaxy groups.

The initial argument for the early formation of fossils relied on the relaxed X-ray morphology, absence of recent mergers and the large gap (2 mag) in the optical luminosity function of their constituent galaxies. Their mass distribution, and in particular their mass concentration parameter, can provide more solid and independent evidence for their early formation. Wechsler et al. (2002) show that halos which have not had a major merger since z = 2 are more concentrated in comparison to systems which had experienced a major merger since then. We measure c_{200} and find that the mass concentration for this system is relatively high compared to clusters of similar mass (Pratt & Arnaud 2005). This is excluding the stellar mass contribution to the total gravitational mass from the central giant elliptical galaxy. We have already reported a very high mass concentration parameter for NGC 6482 (Khosroshahi, Jones & Ponman 2004). In addition, Sun et al. (2004) find a high mass concentration (~ 8.9) when they fit a NFW profile for ESO 3060170, another massive fossil. If fossils are old systems, their core must have formed in an early stages when the density of matter was higher, resulting in formation of a dense and compact core whilst later accretion of mass builds an extended halo. Relatively higher mass concentration of low mass systems compared to more massive halos are seen in cosmological simulations (Bullock et al. 2001).

The central galaxy in this cluster has discy isophotes despite the fact that majority of giant elliptical galaxies at the cores of clusters and groups show boxy isophotes (Kormendy & Bender 1996). There are other examples of discy isophotes in fossils' central galaxies. NGC 6482 also shows highly discy isophotes. The original fossil, RX J1340+4017 has pure elliptical isophotes. We are currently studying the possibility that this, non-boxy isophotes, is a generic property of giant ellipticals at the core of fossil systems.

A more accurate galaxy luminosity function, compared to the first published for a fossil (Jones etal 2001), is presented in this study. The confirmed members form a LF which is steeper than most of the galaxy luminosity functions presented for the groups. We find $\alpha = -1.23 \pm 0.28$ and $M_R^{\star} =$

-20.40 ± 0.22, by fitting the Schecter function to the LF of the spectroscopically confirmed member galaxies. This agrees well with the results of an independent study of this cluster by Cypriano, Mendes de Oliveira & Sodre Jr. (2006).

Miles et al. (2004) found, in their study of GEMS groups, an interesting feature referred to as "dip" in the optical luminosity function of dim (low velocity dispersion) X-ray groups compared to bright (high velocity dispersion) X-ray groups interpreted as being produced as a result of more efficient galaxy merger in low velocity dispersion groups. Similarly, the main argument behind the lack of bright galaxies in fossils is the merger of $L^\star$ galaxies, but fossils are in general more X-ray luminous than the dim X-ray groups studied by (Miles et al. 2004). The velocity dispersion of galaxies in this fossil cluster is $\sigma \approx 700$ km s^{-1} which is consistent with the value expected from the observed cluster L_X-σ (Mahdavi & Geller 2001) given the X-ray luminosity of this cluster. Similarly J1552.2+2013, lies on the same L_X-σ relation (Mendes de Oliveira, Cypriano & Sodre Jr. 2005), though the scatter in the L_X-σ relation is large.

An especially interesting feature of RX J1416.4+2315 is the large size and mass of the system. Dynamical friction, the key process believed to be responsible for the orbit decay which allows the major galaxies to merge within fossil groups, is much less effective at high velocities, raising the question of whether the existence of such a fossil cluster poses a problem for the whole model of fossil system formation through galaxy merging. Jones et al. (2000) estimated the time-scale of dynamical friction for the original fossil group, J1340.6+4018, and showed that $L^\star$ galaxies, initially in circular orbits at half the virial radius and circular velocity of $\sqrt{2}\sigma$, should merge into the central galaxy in 4.5×10^9 yr. The subject of this study, J1416, is more massive and has a radial velocity dispersion, σ almost twice that of J1340.6+4018. It also has a larger virial radius. The time scale for orbital decay of a body of mass M by dynamical friction is proportional to $\frac{r^2 v_c}{M}$, (Binney & Tremaine 1987), which means that a $L^\star$ galaxy in this system will require a dynamical friction time-scale larger than a Hubble time to merge. We note, however, that this estimate is based on initial conditions in which the galaxy is part of a virialised system and rotates on a circular orbit around the centre. If instead, galaxies fall into the developing cluster along a filament, the loss of the angular momentum could occur in a much shorter time, due to the small pericentre radius of their orbits. The X-ray emission, and hence the dark matter distribution in J1416, is highly elongated, implying a very anisotropic velocity dispersion tensor, and supporting the idea of collapse along a dominant filament.

Recent simulations of the formation of fossil systems also suggest that they can be formed with high masses. D'Onghia et al. (2005) find that fossil groups have already assembled half of their final mass at z$\sim$1, and subsequently they typically grow by minor merging only. The early assembly of fossils groups leaves sufficient time for $L^\star$ galaxies to merge into the central galaxy by dynamical friction, resulting in the large magnitude gap.

We would like to thank *Chandra* and *XMM-Newton* observatory teams and the anonymous referee for helpful comments and suggestions that improved the presentation of the paper. We also would like to thank John Mulchaey for his involvement in spectroscopic observations of the target and Issac-Newton group of telescopes for service observation of the target with INT. BJM is supported by NASA through Chandra Postdoctoral Fellowship Award Number PF4-50034 issued by the Chandra X-ray Observatory Center, which is operated by the Smithsonian Astrophysical Observatory for and on behalf of NASA under contract NAS8-03060.

REFERENCES

Arnaud M. et al. , 2002, A&A, 390, 27
Bender R., Burstein D., Faber S. M., 1992, ApJ, 399, 462
Binney J. and Tremaine S., 1987, Galactic Dynamics. Princeton Univ. Press, Princeton, NJ
Bullock J. S., Kolatt T. S., Sigad Y., Somerville R. S., Kravtsov A. V., Klypin A. A., Primack J. R., Dekel A., 2001, MNRAS, 321, 559
Buote D. A. and Canizares C. R., 1996, ApJ, 457, 565
Cappellari M. et al. , 2005, astro-ph/0505042
Carlberg, R. G., et al. 1996, ApJ, 462, 32
Cypriano E. S., Mendes de Oliveira C. & Sodre Jr. L., 2006, submitted to AJ
D'Onghia E., Sommer-Larsen J., Romeo A. D., Burkert A., Pedersen K., Portinari L., Rasmussen J., 2005, ApJ, 630, L109
Dubinski, J. 1998, ApJ, 502, 141
Fabricant D., Rybicki G., Gorenstein P. 1984, ApJ, 286, 186
Girardi M., Manzato P., Mezzetti M., Giuricin G., Limboz F. 2002 ApJ, 569, 720
Jones L. R., Ponman T. J., Horton A., Babul A., Ebeling H., Burke D. J., 2003, MNRAS, 343, 627
Jones L. R., Ponman T. J., Forbes D. A., 2000, MNRAS, 312, 139
Jones L. R., Scharf C., Ebeling H., Perlman E., Wegner G., Malkan M., Horner D. 1998, ApJ, 495, 100
Kazantzidis S., Zentner A. R., Nagai D. 2005, astro-ph/0508114
Khosroshahi H. G., Jones L. R., Ponman T. J., 2004, MNRAS, 349, 1240
Khosroshahi H. G., Raychaudhury S., Ponman T. J., Miles T., Forbes D. A., 2004, MNRAS, 349, 527
Kormendy J. and Bender R., 1996, ApJ, 464, 119
Mahdavi A. and Geller M. J., 2001, ApJ, 554, 129
Matsushita K., 2001, ApJ, 547, 693
Mendes de Oliveira C., Cypriano E. S., Sodre Jr. L., 2005, astro-ph/0509884
Miles T. A., Raychaudhury S., Forbes D. A., Goudfrooij P., Ponman T. J., Kozhurina-Platais V., 2004, MNRAS, 355, 785
Mohr J. J., Geller M. J., Fabricant D. G., Wegner G., Thorstensen J., Richstone D. O., 1996, ApJ, 470, 724
Mulchaey J. S., Zabludoff A. I., 1999, ApJ, 514, 133
Navarro J. F., Frenk C.S., White S. D. M., 1995, MNRAS, 275, 56
Neumann D. M., Böhringer H., 1995, A&A, 301, 865
Perlman E. S., Horner D. J., Jones L. R., Scharf C. A., Ebeling H., Wegner G., Malkan M., 2002, ApJS, 140, 265
Ponman T. J., Allan D. J., Jones L. R., Merrifield M., MacHardy I. M., 1994, Nature, 369, 462
Ponman T. J., Sanderson A. J., Finoguenov A., 2003, MNRAS, 343, 331
Pratt G. W., Arnaud M., 2005, A&A, 429, 791
Pratt G. W., Arnaud M., 2003, A&A, 408, 1
Pratt G. W., Arnaud M., 2003, A&A, 394, 375
Read A. M. and Ponman T. J., 2003, A&A, 409, 395
Romer A. K. et al. , 2000, ApJS, 126, 209
Scharf C. A., Jones L. R., Ebeling H., Perlman E., Malkan M., Wegner G., 1997, ApJ, 477, 79
Smith R. K., Brickhouse N. S., Liedahl D. A., Raymond J. C., 2001, ApJ, 556, L91
Sun M., Forman W., Vikhlinin A., Hornstrup A., Jones C., Murray S. S., 2004, ApJ, 612, 805
Vikhlinin A., McNamara B. R., Hornstrup A., Quintana H., Forman W., Jones C., Way M. 1999, ApJ, 520, 1

Vikhlinin A., Kravtsov A., Forman W., Jones C., Markevitch M., Murray S. S., Van Speybroeck L., 2005, astro-ph/0507092
Wechsler R. H., Bullock J. S., Primack J. R., Kravtsov A. V., Dekel A., 2002, ApJ, 568, 52
Yoshioka T., Furuzawa A., Takahashi S., Tawara Y., Sato S., Yamashita K., Kumai Y., 2004, Adv. in Space Res, 34, 2525

This paper has been typeset from a TEX/ LATEX file prepared by the author.